Fully three-dimensional ideal magnetohydrodynamic stability analysis of low-n modes and Mercier modes in stellarators

G. Y. Fu, W. A. Cooper, and R. Gruber
Centre de Recherches en Physique des Plasmas, Association Euratom-Confédération Suisse,
Ecole Polytechnique Fédérale de Lausanne, Lausanne, Switzerland

U. Schwenn
Max-Planck-Institut für Plasmaphysik, Euratom-IPP Association, Garching, Germany

D. V. Anderson
National Energy Research Supercomputer Center, Lawrence Livermore National Laboratory,
Livermore, California 94550

The TERPSICHORE three-dimensional linear ideal magnetohydrodynamic (MHD) stability code [*Theory of Fusion Plasmas*, Proceedings of the Joint Varenna–Lausanne International Workshop, Chexbres, Switzerland, 1988 (Editrice Compositori, Bologna, Italy, 1989), p. 93; *Controlled Fusion and Plasma Heating*, Proceedings of the 17th European Conference, Amsterdam, The Netherlands (European Physical Society, Petit-Lancy, Switzerland, 1990), Vol. 14B, Part II, p. 931; *Theory of Fusion Plasmas*, Proceedings of the Joint Varenna–Lausanne International Workshop, Valla Monastero, Varenna, Italy, 1990 (Editrice Compositori, Bologna, Italy, 1990), p. 655] has been extended to the full MHD equations. The new code is used to calculate the physical growth rates of nonlocal low-n modes for $l = 2$ torsatron configurations. A comprehensive investigation of the relation between the Mercier modes and the low-n modes has been performed. The unstable localized low-n modes are found to be correlated with the Mercier criterion. Finite growth rates of the low-n modes correspond to finite values of the Mercier criterion parameter. Near the Mercier marginal stability boundary, the low-n modes tend to be weakly unstable with very small growth rates. However, the stability of global-type low-n modes is found to be decorrelated from that of Mercier modes. The low-n modes with global radial structures can be more stable or more unstable than Mercier modes.

I. INTRODUCTION

With the resurgence of interest in stellarator confinement systems, extensive theoretical work has been done on ideal magnetohydrodynamic (MHD) stability of three-dimensional (3-D) stellarator plasmas.[1-3] One of the main focuses of the work is to investigate the relation between low-n modes and Mercier modes,[4-8] where n is the toroidal mode number. These ideal MHD modes impose a stability limit on the plasma beta value, where beta is the ratio between the plasma energy and the magnetic field energy. It is natural to ask which type of mode gives a more stringent stability limit.

Mercier modes are localized to any magnetic rational surface within the plasma. Their stability can be determined by the Mercier criterion[9] for a given magnetic surface. It is also known that low-n ideal MHD modes are often fairly localized around the rational surfaces in stellarators. One may ask whether low-n modes are unstable when the Mercier criterion indicates instability, or vice versa. For example, when the $\iota = 0.5$ magnetic surface is unstable to Mercier modes, is the $(n,m) = (1,2)$ mode unstable, too? Here ι is the rotational transform of the magnetic field line and n/m is the toroidal/poloidal mode number.

In earlier work, Gruber *et al.*[4] and Merkel *et al.*[5] compared unstable regions and beta limits for low-n modes and Mercier modes for helically symmetric equilibria, using their helically symmetric version of the ERATO stability

code,[10] namely HERA.[11] It was found that when low-n modes were unstable, the Mercier modes were also unstable at the corresponding magnetic rational surfaces. Sugama and Wakatani[6] studied the nature of Mercier modes and low-n modes more precisely, but for a one-dimensional model. They found that the growth rate of low-n modes approached the analytic growth rate of Suydam modes (or Mercier modes) as the mode number increases, with the mode helicity fixed. It was also found that the growth rate curves of both Mercier modes and low-n modes as functions of the plasma beta were very flat near the critical beta value. More recently, Dominguez *et al.*[7] extended these comparisons to 3-D $l = 2$ torsatron equilibria. They found that the low-n modes corresponding to resonant surfaces unstable to Mercier modes were also unstable in most cases studied and that the Mercier criterion imposes a slightly lower critical beta. In their calculations, the Mercier criterion was evaluated in fully 3-D equilibria, but the low-n modes were computed using the stellarator expansion method,[12,13] which reduces the problem to two dimensions by averaging over the fast helical variations of the magnetic fields. Nakamura *et al.*[8] applied a more consistent method using the same stellarator expansion code, STEP,[14] to calculate both the equilibrium and the stability of low-n modes and Mercier modes. A more definite correlation between the low-n modes and Mercier modes was found. The low-n modes were predicted to be

unstable whenever $D_M \leqslant -0.2$, where D_M is the Mercier parameter, whose shear-squared term is normalized as $1/4$.

Most of the previous work was not fully three dimensional. The stellarator expansion method was used in studying the low-n modes, which is only valid in the limit of large aspect ratio, large number of field periods, and planar magnetic axis. It is of interest to see whether a fully 3-D calculation could modify some of the results. Recently, efficient 3-D ideal MHD stability codes for nonlocal modes have become available.[15-19] A few examples of fully 3-D studies of low-n modes and Mercier modes have been given.[19,20] However, a comprehensive study of the relation between low-n modes and Mercier modes is still lacking for fully 3-D calculations.

In this work, we extend previous work to a fully 3-D calculation and systematically compare the MHD stability of low-n modes with those of Mercier modes for a sequence of $l = 2$ equilibria. The equilibria used were calculated with the VMEC 3-D code.[21,22] The Mercier criterion is evaluated in Boozer coordinates.[23] To facilitate our calculation of low-n modes, we extend the original version of the TERPSICHORE 3-D ideal MHD stability code[15-17] to the full MHD equations. In the previous versions of the TERPSICHORE code, the incompressibility condition $\nabla \cdot \xi = 0$ was imposed, and a model kinetic energy term was adopted. Another 3-D ideal MHD code,[18,19] namely CAS3D,[19] also used the same model. This model reduces the MHD equations to only two components of the perturbed plasma displacement vector. The stability marginal points are unchanged, but the physical growth rates cannot be calculated. This limitation is eliminated in our new version of the TERPSICHORE code. Because we concentrate on the relation between the Mercier modes and internal low-n modes in this paper, we exclude free boundary modes from the analysis, which can impose more restrictive stability limits for global-type modes.[20,24]

The paper is organized as follows. In Sec. II, we sketch the extension of the original version of TERPSICHORE to the full MHD model and give benchmark results. In Sec. III, we present applications of our code to fully 3-D geometry and present the numerical methods. Section IV is devoted to the studies of low-n modes and Mercier modes. Finally in Sec. V we give conclusions.

II. THE TERPSICHORE LINEARIZED FULLY IDEAL MHD CODE

A. Description of the code

The new TERPSICHORE code solves the linearized ideal MHD equations in variational form for 3-D stellarator configurations. The linearized MHD equation can be expressed in the variational form:

$$\delta W_p + \delta W_v - \omega^2 \delta W_k = 0, \tag{1}$$

where δW_p is the perturbed potential energy of the plasma, δW_v is the perturbed magnetic energy in the vacuum region that surrounds the plasma, $-\omega^2 \delta W_k$ is the perturbed kinetic energy of the plasma, and ω is the frequency of the perturbation. These terms can be written as

$$\delta W_p = \frac{1}{2} \int \int \int d^3x [C^2 + \Gamma p |\nabla \cdot \xi|^2 - D |\xi \cdot \nabla s|^2], \tag{2}$$

$$\delta W_v = \frac{1}{2} \int \int \int d^3x |\nabla \times A|^2, \tag{3}$$

$$\delta W_k = \frac{1}{2} \int \int \int d^3x \rho |\xi|^2, \tag{4}$$

with the vector

$$C = \nabla \times (\xi \times B) + \frac{j \times \nabla s}{|\nabla s|^2}(\xi \cdot \nabla s) \tag{5}$$

and the coefficient

$$D = \frac{2(j \times \nabla s) \cdot (B \cdot \nabla) \nabla s}{|\nabla s|^4}, \tag{6}$$

where ρ is the plasma mass density, ξ is the perturbed plasma displacement vector, Γ is the adiabatic index, p is the plasma pressure, s is the magnetic flux variable, B is the equilibrium magnetic field, j is the equilibrium plasma current density, and A is the potential of the perturbed magnetic field in the vacuum region. The equilibrium is obtained with the VMEC 3-D code and is mapped to Boozer coordinates, for which the magnetic field lines are straight and the Jacobian of the coordinate transformation $\sqrt{g}$ is proportional to $1/B^2$. The displacement vector ξ is decomposed in the following way:

$$\xi = \sqrt{g}\xi^s \nabla \theta \times \nabla \phi + \eta[(B \times \nabla s)/B^2] + \mu B, \tag{7}$$

where $\xi^s = \xi \cdot \nabla s$ is the normal component, η and μ are two components in the magnetic flux surfaces, and θ /ϕ is the poloidal/toroidal angle variable. These three components are expanded in a truncated Fourier series

$$\xi^s(s,\theta,\phi) = \sum_l \xi_l(s)\sin(m_l\theta - n_l\phi + \Delta), \tag{8}$$

$$\eta(s,\theta,\phi) = \sum_l \eta_l(s)\cos(m_l\theta - n_l\phi + \Delta), \tag{9}$$

$$\mu(s,\theta,\phi) = \sum_l \mu_l(s)\cos(m_l\theta - n_l\phi + \Delta), \tag{10}$$

where subscript l denotes the lth Fourier component and Δ is an arbitrary phase factor. The boundary conditions at the magnetic axis $s = 0$ are regularized by the transformation $\xi_l(s) \rightarrow s^{q_l}\xi_l(s)$. Piecewise linear finite elements are used to represent $\xi_l(s)$, and piecewise constant elements are used to represent $\eta_l(s)$ and $\mu_l(s)$. After the integration in θ, ϕ, and s is carried out, the energy principle reduces to the matrix equation

$$\mathscr{A}x = \omega^2 \mathscr{B}x, \tag{11}$$

where $\mathscr{A}$ is the potential energy matrix, $\mathscr{B}$ is the kinetic energy matrix, x is the eigenfunction, and ω^2 is the eigenvalue. In the eigenvalue problem, negative eigenvalues correspond to unstable modes. The matrices $\mathscr{A}$ and $\mathscr{B}$ have block diagonal structures. This matrix equation is solved with an iterative scheme.[18]

1402   Phys. Fluids B, Vol. 4, No. 6, June 1992

Fu et al.   1402

B. Benchmark of the code

We first compare the stability results of our code with those of other known results for two-dimensional (2-D) analytic Solov'ev equilibria.[25] This tokamak equilibrium is described by the poloidal flux function

$$\Psi(R,Z) = \frac{\Psi_1}{a^2 R^2}\left(\frac{R^2 Z^2}{E^2} + \frac{(R^2 - R_0^2)^2}{4}\right), \quad (12)$$

where Ψ_1 is the total poloidal flux within the plasma, R and Z are the cylindrical coordinates, R_0 is the radius of the magnetic axis, a is a measure of the minor radius, and E is the elongation of the plasma flux surfaces. The equilibrium is fully defined by three parameters: the aspect ratio R_0/a, elongation E, and the safety factor on the axis $q(0)$. Here we consider the equilibria with $R_0/a = 3$. Table I lists the normalized eigenvalues γ/ω obtained with our code and two other codes, ERATO (Ref. 10) and MARS,[26] for three Solov'ev equilibria, where $\gamma^2 = -\omega_A^2$ and the normalizing Alfvén frequency ω_A is defined as $\omega_A = V_A/R_0$, with V_A being the Alfvén phase velocity, and n is the toroidal mode number. Our results were obtained by extrapolating to zero radial mesh size and by using a sufficient number of Fourier modes. Fixed boundary conditions were used. We note that our results agree very well with those of the ERATO and MARS codes.

We now consider a straight $l = 2$, $M = 5$ stellarator with helical aspect ratio $A_h = 2\pi r_b/L = 1.51$,[15,27] where r_b is the mean radius of the plasma boundary and L is the length of the equilibrium period. This equilibrium is nontrivial for benchmarking of our code since there is mode coupling between different toroidal mode numbers in Boozer coordinates, just as in fully 3-D equilibria. The stability results of an $n = 1$, $m = 2$ mode have already been computed[27] with the BETA nonlinear 3-D code, the HERA code, and the STEP code. Figure 1 shows the normalized eigenvalue $-\omega^2/\omega_A^2$ as a function of the rotational transform on the magnetic axis ι_0 from various codes for a case with volume-averaged beta $\beta = 3\%$. We observe that our results agree relatively well with the others. The small discrepancy in the eigenvalues may be attributed to the different ways of specifying the equilibria used in these computations. In our calculation, the equilibria were computed with the VMEC code with a pressure profile $p(s) = p(0)(1 - s)$ and a density profile $\rho(s) = \rho(0)\sqrt{1 - s}$, and the adiabatic index was taken to be $\Gamma = 5/3$. The radial flux variable s was chosen proportional to the toroidal flux Φ. The radial resolution and the number of Fourier modes were sufficient to obtain converged eigenvalues.
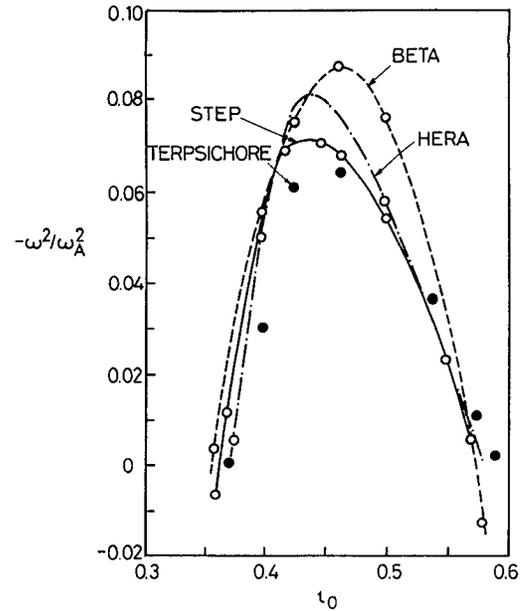

FIG. 1. Growth rates for an $n = 1$, $m = 2$ instability in a straight $l = 2$, $M = 5$ helical system obtained with the BETA (dashed line), HERA (broken line), STEP (solid line), and TERPSICHORE (solid dots) codes as a function of the rotational transform at the magnetic axis.

III. APPLICATION TO FULLY 3-D STELLARATOR EQUILIBRIA

A. Equilibrium

We consider $l = 2$ torsatron configurations with zero net toroidal current. Each equilibrium is specified by the number of field periods N_p, the plasma boundary, the pressure profile, and the volume-averaged beta β. We define our plasma boundary in cylindrical coordinates (R,Z) with a truncated Fourier series

$$R(\theta,\phi) = \Sigma_{m,n} R_{m,n} \cos(m\theta - nN_p\phi), \quad (13)$$

$$Z(\theta,\phi) = \Sigma_{m,n} Z_{m,n} \sin(m\theta - nN_p\phi). \quad (14)$$

We note that the zero beta equilibrium is solely determined by the plasma boundary for fixed N_p. The equilibrium can be varied by changing these boundary Fourier coefficients. Physically, the coefficient $R_{0,0}$ is a measure of the radius of the magnetic axis, $R_{1,0}$ is a measure of the plasma mean radius, $R_{1,1}$ and $Z_{1,1}$ control the strength of the main helical field, and $R_{2,1}$ and $Z_{2,1}$ can control the position of the magnetic axis. We define our equilibrium sequence, using the following set of Fourier coefficients: $R_{0,0}$, $R_{1,1} = -Z_{1,1}$, and $R_{2,1} = -Z_{2,1}$, with $R_{1,0} = 0.22$ and $Z_{1,0} = 0.25$ being fixed. Other coefficients are chosen to be zero. Table II lists the set of Fourier coefficients for the equilibria to be studied. The pressure profile is prescribed to be $p(s) = p(0)(1 - 3s^2 + 2s^3)$ with vanishing gradient at $s = 0$ and $s = 1$, except when otherwise mentioned. The radial variable is chosen to be proportional to the toroidal flux.

The VMEC code was used to obtain every equilibrium used in our calculations. We chose a set of Fourier modes with $0 \leqslant m \leqslant 5$ and $-3N_p \leqslant n \leqslant 3N_p$ and used up to 96 radial

TABLE I. Normalized growth rates γ/ω_A from the ERATO, MARS, and TERPSICHORE codes for Solov'ev equilibria.

n	$q(0)$	E	ERATO	MARS	TERPSICHORE
2	0.3	2	1.26	1.26	1.25
2	0.7	2	0.284	0.284	0.284
3	0.75	1	0.0541	0.0533	0.0538

TABLE II. Plasma boundary Fourier coefficients and number of field periods for our equilibrium sequence.

| Equilibrium	$R_{0,0}$	$R_{1,1}$	$R_{2,1}$	N_p
S	2.1	−0.07	−0.01	12
A	1.8	−0.07	−0.01	12
B	1.5	−0.07	−0.01	12
C	2.1	−0.07	−0.02	12
D	2.1	−0.06	−0.02	12
E	2.1	−0.07	−0.02	18
F	2.1	−0.07	−0.02	10

FIG. 2. Eigenvalues of an $n = 3$ unstable mode as a function of the radial mesh size squared h^2 for three values of the integration parameter α, for the equilibrium A at $\beta = 1.58\%$.

grid points. We found this resolution to be sufficient to obtain converged equilibria.

B. The tunable integration method

It is well known that the piecewise finite element method leads to quadratic convergence for the eigenvalue of a second-order differential equation. Indeed, our code observes this known scaling. The original version of the TERPSICHORE code used the so-called finite hybrid element method (FHM),[7] where the radial integration was carried out with a midpoint rule. FHM is very well tailored to ideal MHD stability problems and has fast radial convergence. But this method destabilizes the stable shear Alfvén continuum, whose eigenvalues often mask the small physical eigenvalues. This destabilization can be solved in a cumbersome way by adding a large number of grid points or by accumulating grid points around each of the resonant surfaces present. We solve this problem with the tunable integration method (TIM),[28] which has been implemented and tested in our code. TIM only differs from FHM in the way the numerical radial integration is performed. It uses the following integration scheme:

$$\int_{s_i}^{s_{i+1}} I(s)ds = (s_{i+1} - s_i)\left[(1-\alpha)I\left(\frac{s_i + s_{i+1}}{2}\right)\right.$$
$$\left. + \frac{\alpha}{2}[I(s_i) + I(s_{i+1})]\right], \quad (15)$$

where $I(s)$ represents the integrand in the energy principle, the subscript s_i denotes the value of s at the ith grid, and α is a parameter to be varied from 0 to 1. Note that $\alpha = 0$ (midpoint rule) corresponds to the FHM, $\alpha = 1/3$ (Simpson's rule) corresponds to the strict finite element method, and $\alpha = 1$ (trapezoidal rule) corresponds to the finite-difference method. The basic ideal of TIM is to control the total discretization error by varying the numerical integration error through the continuous parameter α.

Figure 2 shows the eigenvalue ω^2/ω_A^2 versus the square of the radial mesh size for different values of the parameter α, for equilibrium A with $\beta = 1.58\%$. The calculation was done with uniform radial grid points. It is clear that convergence is quadratic for every value of the parameter α. Note that the eigenvalue with $\alpha = 0$ (i.e., FHM) converges from
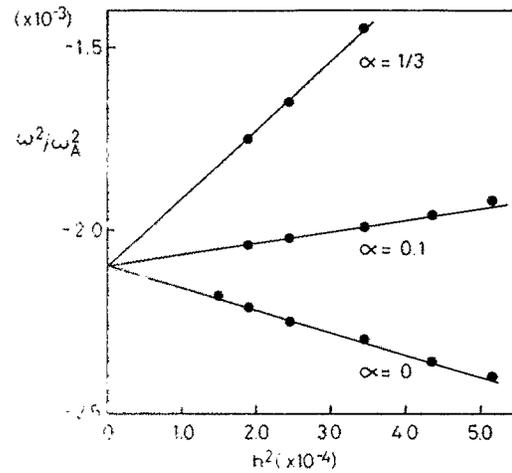
below (the unstable side), and the one with $\alpha = 1/3$ converges from above (stable side). A smaller value of $\alpha = 0.1$ produces the best convergence from above. It should be noted that all the eigenvalues converge to the same value. We now show an example of destabilization of the continuum modes by the FHM (corresponding to $\alpha = 0$). We consider the equilibrium A with $\beta = 1.02\%$, for which the $n = 3$ mode is weakly unstable. Figure 3 shows (a) the first most unstable mode and (b) the second most unstable mode. Since the mode was localized around the $\iota = 3/4$ rational surface, half of the total 48 grid points were accumulated around that surface. We see that the first mode has a singular structure in the eigenfunction around the rational surface $\iota = 1$, signifying a continuum mode destabilized by the FHM. The second mode has a regular mode structure peaked at the $\iota = 3/4$ surface and is physical, with its eigenvalue $-\omega^2/\omega_A^2 = 1.12 \times 10^{-4}$ masked by the first unphysical eigenvalue $-\omega^2/\omega_A^2 = 3.05 \times 10^{-4}$. However, when TIM is applied with $\alpha = 0.05$, the most unstable mode is found to be physically the same as the second most unstable mode found with the FHM, but with an eigenvalue $-\omega^2/\omega_A^2 = 7.63 \times 10^{-5}$. This means that the numerically unstable continuum mode is restabilized by our new method. We conclude that the tunable integration method is useful for obtaining fast convergence without numerical destabilization of the singular continuum modes.

C. Convergence in the number of Fourier modes

Having considered the convergence in the radial direction, we now discuss the convergence in the poloidal and the toroidal domains. Since Fourier decomposition is used in the angle variables, we discuss the convergence in the number of Fourier modes. Before going into details, we first discuss the mode selection. In 3-D geometry, the toroidal mode number is no longer a good "quantum number," unlike in the case of axisymmetric tokamak equilibrium. Therefore, modes with
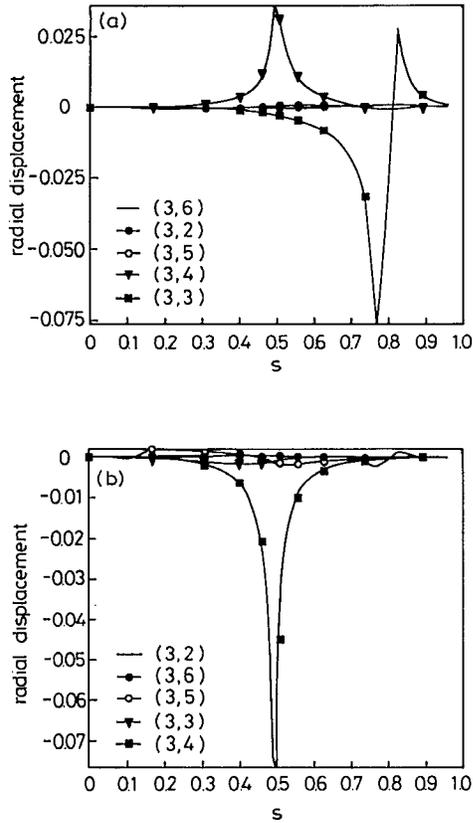
FIG. 3. The radial displacement functions $\xi_l(s)$ of (a) the most unstable $n = 3$ mode and (b) the second most unstable $n = 3$ mode for equilibrium A at $\beta = 1.02\%$. Different Fourier components are marked by (n,m), where n/m is the toroidal/poloidal mode number.

number of Fourier modes. We consider the $n = 3$ family for our standard equilibrium S. Figure 4(a) shows the rotational transform profile $\iota(s)$ at $\beta = 2.36\%$. Since the rational surface $\iota = 3/4$ is in the magnetic hill region for the corresponding vacuum state, we expect the $n = 3$ family of the eigenmodes to be unstable, with $(3,4)$ as the dominating Fourier component. Indeed, it was found to be unstable, with its eigenmode structure localized around the $\iota = 3/4$ rational surface as shown in Fig. 4(b). Figure 5(a) shows the eigenvalue $-\omega^2/\omega_A^2$ as a function of $1/N$, where N is the number of Fourier modes used. Recall that the convergence depends on ways of selecting Fourier modes for a given N. Our selection for $N = 24$ is $-1 \leqslant m \leqslant 10$ for $n = 3$, $0 \leqslant m \leqslant 5$ for $n = -9$, and $4 \leqslant m \leqslant 9$ for $n = 15$. From 24 modes to 36 modes, we increased N by adding two modes to each n, and from 36 modes to 54 modes by adding three modes to each of the toroidal sidebands $n \pm 2N_p$. The result was obtained with 48 uniform radial grid points and with the integration parameter $\alpha = 0$ for two different values of the adiabatic index Γ. We observe in Fig. 5(a) that the convergence with $\Gamma = 5/3$ is slower than with $\Gamma = 0$. In particular, the eigenmode is stable for 24 modes. A more dramatic example is shown in Fig. 5(b) for equilibrium C. The unstable eigenmode is very global with strong poloidal mode coupling, as shown in Fig. 6(a), in contrast with the less global

different toroidal numbers n are coupled to each other. Nonetheless, the stellarator geometry still has some degree of symmetry, i.e., going around in the toroidal direction, the configuration repeats itself N_p times. As a consequence, the modes with toroidal number n are only coupled to modes with n, $n \pm N_p$, $n \pm 2N_p$, and $n \pm 3N_p$, etc. There are a total of $N_p/2$ families [$(N_p - 1)/2$ families] of modes for configurations with even (odd) number of field periods, excluding the modes that describe the equilibrium state. Each family has to be computed in order to have a complete picture of the MHD stability behavior. Furthermore, there is usually more than one unstable eigenmode with the same or different dominating Fourier component (n,m) within each family. For our purpose, we will only consider four families of the mode with $1 \leqslant n \leqslant 4$ as the dominating toroidal number. Once the main n is chosen, there is still a question of mode selection, i.e., how to select the poloidal modes for each n. We have found that, for $l = 2$ torsatrons, the dominating poloidal harmonic of an unstable eigenmode is approximately $\overline{m} \pm 2k$ for the toroidal sidebands $\overline{n} \pm kN_p$, where k is an integer and $(\overline{n},\overline{m})$ is the main component. Thus, we distribute poloidal modes evenly around these dominating $\overline{m} \pm 2k$. This way of mode selection was found to be nearly optimal.

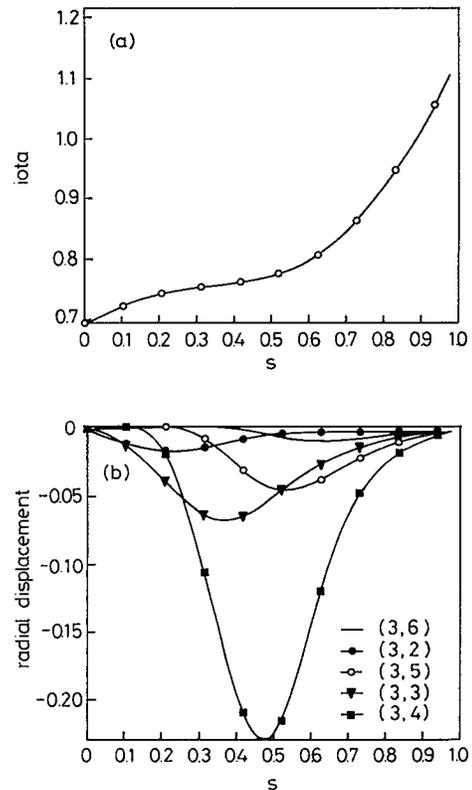We now discuss the behavior of the convergence in the

FIG. 4. The equilibrium rotational transform profile and the corresponding $n = 3$ unstable mode: (a) profile of the rotational transform $\iota(s)$ and (b) the radial displacement functions of an unstable $n = 3$ mode for the equilibrium A at $\beta = 2.36\%$.
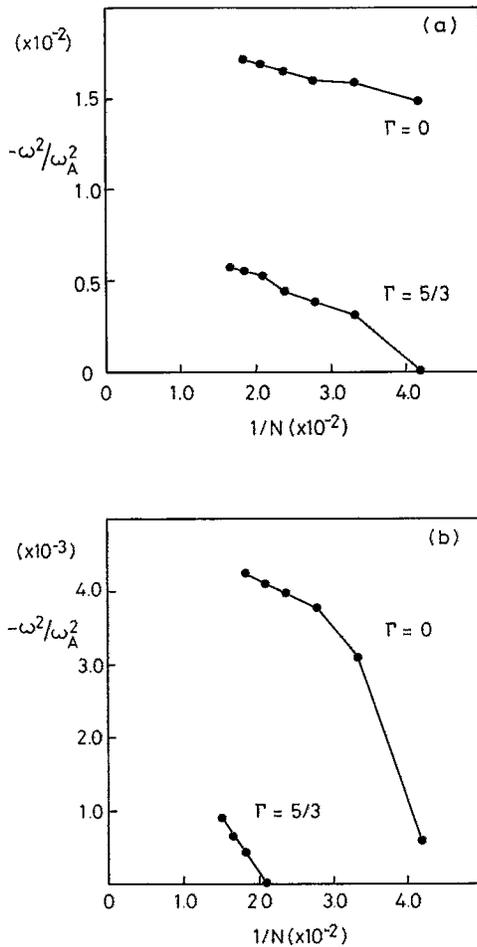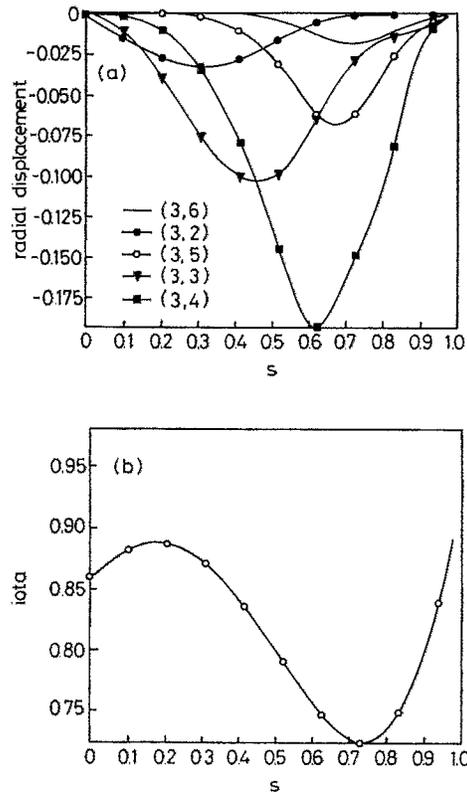
FIG. 6. (a) The radial displacement functions of an unstable $n = 3$ mode obtained with 36 Fourier modes for the equilibrium C at $\beta = 3.48\%$ and (b) the corresponding rotational transform profile of the equilibrium.

FIG. 5. Eigenvalues of unstable $n = 3$ modes as functions of $1/N$ for two values of the adiabatic index $\Gamma = 0$ and $\Gamma = 5/3$, where N is the number of Fourier modes: (a) the eigenvalues obtained with the equilibrium A at $\beta = 2.36\%$ and (b) the eigenvalues obtained with the equilibrium C at $\beta = 3.48\%$.

mode of Fig. 4(b). The corresponding rotational transform profile of the equilibrium is shown in Fig. 6(b). For $\Gamma = 0$, the eigenvalue is nearly converged, but for $\Gamma = 5/3$ there is no sign of convergence up to 66 modes. The reasons for the different convergence behavior are twofold. First, the mode spectrum is broadened by the coupling of shear Alfvén waves and sound waves due to nonzero Γ. Second, the $\nabla \cdot \boldsymbol{\xi}$ term in the energy principle cannot be made as small as it should be owing to the insufficient number of modes resulting from mode coupling. Stated more explicitly, the compression term cannot be made zero for a finite number of Fourier modes. As a consequence, unstable modes may be stabilized numerically, as shown in Figs. 5(a) and 5(b). In order to show the size of the error in the compression term, we have calculated the correction of the eigenvalue due to the compression term by dropping the μ component in the kinetic energy term. The $\nabla \cdot \boldsymbol{\xi}$ should then be zero since now only this term contains the component μ. Numerically this term is not exactly zero for a finite number of Fourier modes.

Figure 7 shows the correction of the eigenvalue as a function of $1/N$ for the equilibrium of Fig. 5 with $\Gamma = 5/3$. We see that the correction decreases by two orders of magnitude when N increases from 24 to 60. Therefore, it is extremely important to have a sufficient number of Fourier modes in order to obtain convergence in 3-D MHD stability calculations for stellarator plasmas. For this reason, we choose $\Gamma = 0$ for all our subsequent calculations to save computa-
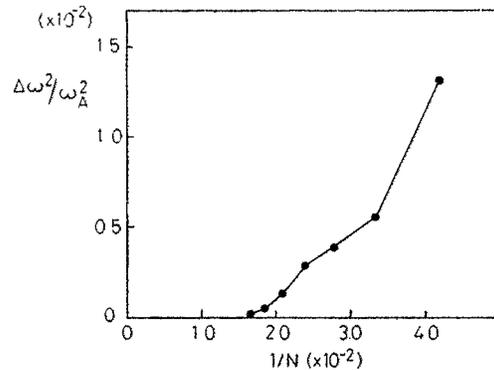

FIG. 7. Correction to the eigenvalue ω^2/ω_A^2 due to the nonzero compressional term being a function of $1/N$ for the same $n = 3$ unstable mode as in Fig. 5.

1406   Phys. Fluids B, Vol. 4, No. 6, June 1992

Fu *et al.*   1406

tional time, since then fewer Fourier modes are needed for convergence. We note the growth rates obtained with $\Gamma = 0$ are somewhat larger than with $\Gamma = 5/3$.

D. The Mercier criterion in Boozer coordinates

The Mercier criterion is a sufficient condition for modes localized around a rational flux surface. We use a convenient form derived by Bauer et al.[29] In Boozer coordinates, this form of the criterion reduces to

$$D_M > 0 \tag{16}$$

for stability, where

$$(\Psi''\Phi')^2 D_M = \left(\frac{\Psi''\Phi'}{2} - \left\langle \frac{\sqrt{g}\mathbf{j}\cdot\mathbf{B}}{|\nabla s|^2} \right\rangle\right)^2 - \sqrt{g}B^2 \left\langle \frac{1}{|\nabla s|^2} \right\rangle$$

$$\times \left(-p'V'' + p'^2 \left\langle \frac{\sqrt{g}}{B^2} \right\rangle \right)$$

$$+ \frac{1}{\sqrt{g}B^2} \left\langle \frac{(\sqrt{g}\mathbf{j}\cdot\mathbf{B})^2}{|\nabla s|^2} \right\rangle \right) \tag{17}$$

where the flux average is $\langle \cdots \rangle = \int\int (\cdots) d\theta\, d\phi/4\pi^2$, Ψ and Φ are the poloidal and toroidal magnetic flux function, respectively, V is the volume of the plasma enclosed by the flux surface labeled with s, and a prime denotes the derivative of a flux surface quantity with respect to s. Note that we have normalized the Mercier parameter D_M in such a way that the shear-squared term is 1/4. We have also imposed the condition of zero net toroidal current and chosen the radial variable s to be proportional to Φ. Finally, the parallel current term can be evaluated through the quasineutrality condition and the MHD equilibrium force balance equation:

$$\mathbf{B}\cdot\nabla(\sqrt{g}\mathbf{j}\cdot\mathbf{B}) = -p'(\mathbf{B}\times\nabla s)\cdot\nabla\sqrt{g}. \tag{18}$$

This form of the Mercier criterion, which has been implemented in our code, is equivalent to a form derived from the ballooning mode equation.[20] It would be instructive to compare the stability of the Mercier modes with that of ballooning modes, but this is beyond the scope of our paper.

IV. IDEAL MHD STABILITY OF LOW-N MODES AND MERCIER MODES

A. Numerical results

In this section, we compare the stability of low-n modes with that of Mercier modes. The Mercier stability is determined at each flux surface according to Eq. (17). The stability of low-n modes is determined by our new TERPSICHORE 3-D stability code. Note that in this section, we have chosen $\Gamma = 0$ to calculate the eigenvalue. Consequently, the values of ω^2/ω_A^2 are somewhat larger than the magnitudes that would result from the conventional definition with $\Gamma = 5/3$. In the computation of low-n modes, small growth rates of $\omega^2/\omega_A^2 \sim 10^{-4}$ were obtained by extrapolating to zero grid size. Up to 96 radial grid points were used. For the poloidal and toroidal resolution, we chose 36 Fourier modes, of which there are 16 poloidal modes for the main n, and ten for each of the two toroidal sidebands $n \pm N_p$. We found this mode selection to be sufficient for the accurate determina-
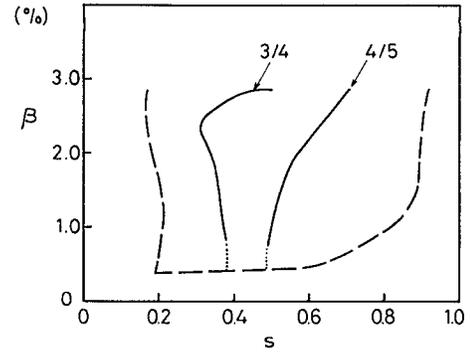

FIG. 8. Mercier stability boundary (dashed line) and unstable range of low-n modes (solid line) for equilibrium S. The Mercier modes are unstable inside the dashed line. The position of each solid line or dotted line indicates the corresponding rational flux surface at which $\iota = n/m$, where n and m represent the dominating toroidal and poloidal mode numbers of the low-n instability, respectively.

tion of the eigenvalues (to within 10% of the converged values) for our purpose. The results were spot-checked by using 60 Fourier modes.

Figure 8 shows the Mercier stability boundary (dashed line) and unstable range of low-n modes in (β,s) space for our standard equilibrium S. Inside the dashed line, the Mercier criterion indicates instability. The unstable ranges of β for low-n modes are indicated by solid lines. The positions in s of the solid lines and the dotted lines indicate the corresponding rational magnetic surfaces. We approximate the marginal points of low-n modes by the condition $-\omega^2/\omega_A^2 = 10^{-4}$. This may be justified because the numerical resolution is limited and because unstable MHD modes with smaller growth rates can easily be stabilized by various kinetic effects neglected in the ideal MHD model. We see in Fig. 8 that when the low-n modes corresponding to the $n = 3$ family and $n = 4$ family are unstable, the Mercier modes are also unstable at the corresponding rational surfaces $\iota = 3/4$ and 4/5. However, there are gaps between the stability limits of the low-n modes and the Mercier modes. For $0.4\% \leqslant \beta \leqslant 0.8\%$, the Mercier modes are unstable while the low-n modes are stable (or marginally unstable with $-\omega^2/\omega_A^2 < 10^{-4}$).

We now look at the stability results of equilibrium A. The equilibrium has a smaller aspect ratio compared with the standard equilibrium S and is obtained by changing the plasma boundary Fourier coefficient $R_{0,0}$ from 2.1 to 1.8. Figure 9 shows a pattern similar to that of Fig. 8. As $R_{0,0}$ is further decreased to 1.5, the resulting equilibrium B has an even smaller Mercier unstable region, as shown in Fig. 10, while the stability of low-n modes becomes somewhat complex. First, the $n = 2$ family is unstable for $\beta \geqslant 2.0\%$ as usual, and there still exists a gap between the marginal point of the $n = 2$ mode and that of the Mercier mode. Second, the $n = 3$ family corresponding to the $\iota = 3/4$ surface is only unstable with a very small range of $2.4\% \leqslant \beta \leqslant 2.8\%$ [i.e., the $n = 3$ eigenmode with the dominating Fourier component (3,4) has a second stable region]. Third, the $n = 3$ mode becomes unstable again for $\beta \geqslant 2.86\%$, but with a different dominat-
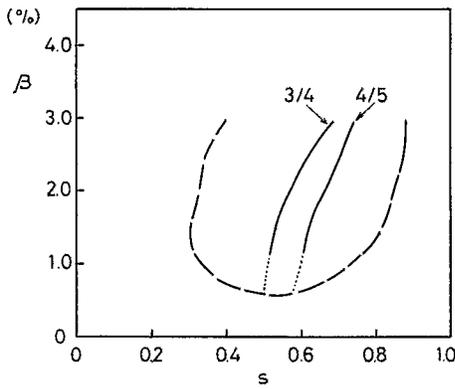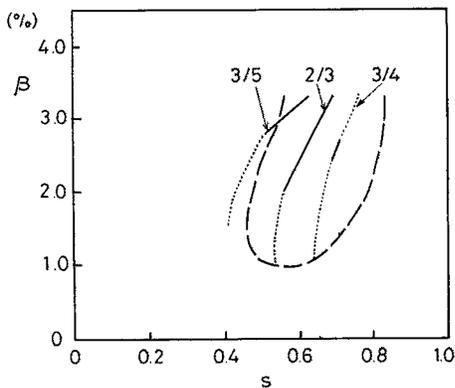
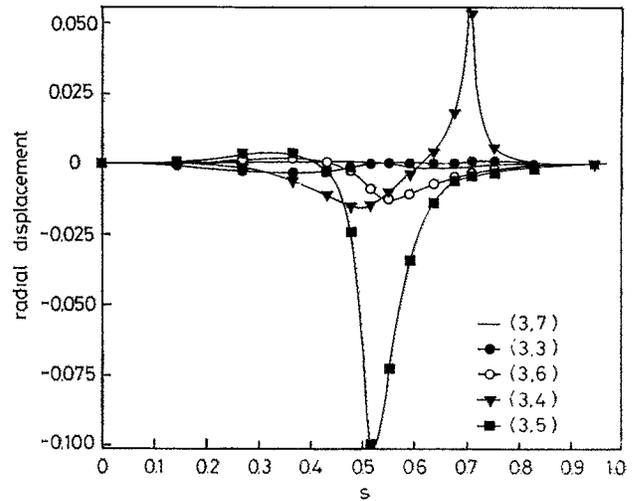FIG. 9. Mercier stability boundary and unstable range of low-n modes, same as in Fig. 8, but for equilibrium A.

FIG. 11. Radial displacement functions of an unstable $n = 3$ mode for equilibrium B at $\beta = 2.75\%$.

ing Fourier component (3,5) corresponding to the $\iota = 3/5$ surface. Notice that near $\beta = 2.90\%$ the (3,5) mode is unstable, but the corresponding $\iota = 3/5$ surface is Mercier stable, i.e., the mode is more unstable than the Mercier mode. This discrepancy may be explained by the fact that the main (3,5) component has a sizable sideband (3,4), as shown in Fig. 11. Presumably, the stability of this multihelicity-type eigenmode cannot be adequately described by the Mercier criterion, for which the eigenmode is constrained to be localized around a single resonance surface.

Figure 12 shows the results for equilibrium C, whose magnetic axis is shifted outward compared with the standard equilibrium S. We see that the $\iota = 3/4$ and $4/5$ rational surfaces are Mercier stable, but the $n = 3$ family is unstable with a dominating (3,4) component, and so is the $n = 4$ family with (4,5) as the main Fourier component. The $n = 3$ and 4 modes are both fairly global, as shown in Fig. 6(a) for the $n = 3$ mode. From Figs. 6(a) and 6(b), we note that these global mode structures concentrate in the region of tokamaklike shear that is induced at finite β in torsatrons with zero net toroidal current. Rewoldt and Johnson[24] identified this type of global mode and its implications on beta

limits for the Advanced Toroidal Facility (ATF) (Ref. 30) using the stellarator expansion method. The fact that these modes have strong poloidal mode coupling with global mode structures explains the discrepancies between their stability and that of Mercier modes. In contrast, Mercier modes are typically very localized with very weak poloidal mode coupling, as shown in Fig. 3(b).

Figure 13 shows results for equilibrium D with small shear. The $n = 2$ family is stable despite the corresponding $\iota = 2/3$ surface being Mercier unstable. The plasma remains stable to both the low-n modes and Mercier modes for $\beta > 2.3\%$ up to the equilibrium limit. For equilibrium E with 18 field periods, the low-n mode $n = 1$ family is again unstable as it is for the Mercier mode at the $\iota = 1$ surface, shown in Fig. 14. Likewise the $n = 2$ family is unstable. There is still a gap between the low-n marginal stability point and the Mercier limit. We have also studied the MHD stability for equilibrium F with ten field periods. Both the low-n modes and

FIG. 10. Mercier stability boundary and unstable range of low-n modes, same as in Fig. 8, but for equilibrium B.
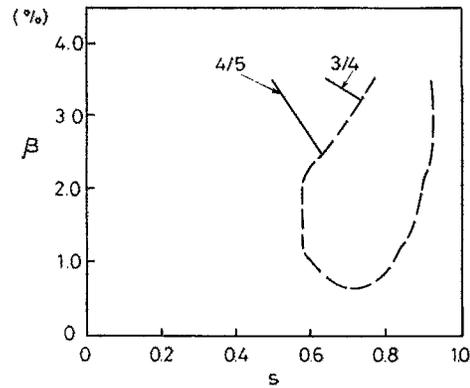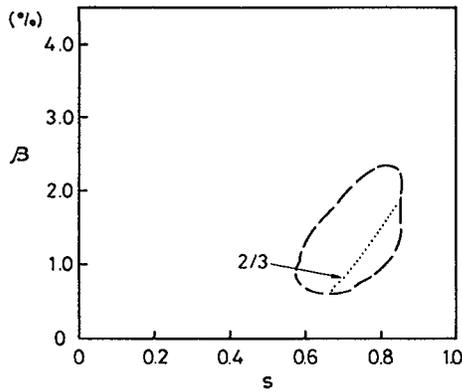

FIG. 12. Mercier stability boundary and unstable range of low-n modes, same as in Fig. 8, but for equilibrium C.

FIG. 13. Mercier stability boundary and unstable range of low-n modes, same as in Fig. 8, but for equilibrium D.
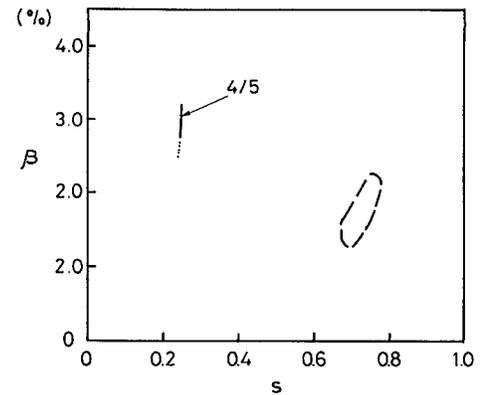

FIG. 15. Mercier stability boundary and unstable range of low-n modes, same as in Fig. 8, but for equilibrium C with peaked pressure profile $p(s) = p(0)(1 - s)^2$.

the Mercier modes were found to be stable up to the corresponding equilibrium limit.

We now study the effects of pressure profiles on the stability of low-n modes and Mercier modes. It is generally agreed that the pressure profile has significant effects. Shown in Fig. 15 are results for the same equilibrium as that of Fig. 12, but with a more peaked profile of $p(a) = p(0)(1 - s)^2$. We see that Mercier modes have only a much smaller unstable region, as compared with that of Fig. 12, and the $n = 4$ mode is unstable at higher beta $\beta > 2.8\%$. The eigenmode is very global and the $\iota = 4/5$ resonant surface of its main Fourier component is located far away from the small Mercier unstable region. Next, we show the results for the standard ATF equilibrium. For our standard pressure profile, there is a narrow Mercier unstable region shown in Fig. 16(a). The $n = 2$ and 3 modes corresponding to the unstable Mercier rational surfaces were found to be stable. Again a global $n = 2$ mode is unstable with its main resonant $\iota = 2/4$ iota surface outside the Mercier unstable region. In contrast, Fig. 16(b) shows that Mercier modes are stabilized for peaked pressure profile with $\beta < 4.3\%$, because the pressure gradient is concentrated in

the region where a magnetic well exists in the vacuum state. The global-type $n = 1$ mode was found to be most unstable. It should be noted that for this particular case the $n = 1$ mode imposes a lower stability beta limit than that of Mercier modes. This feature was previously found in a free
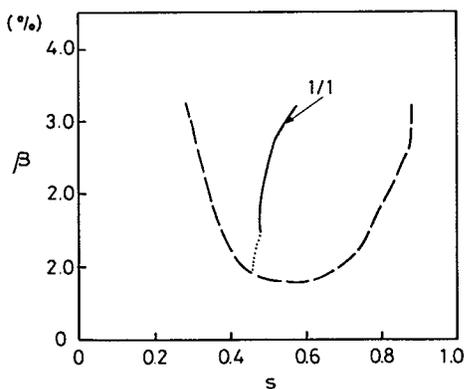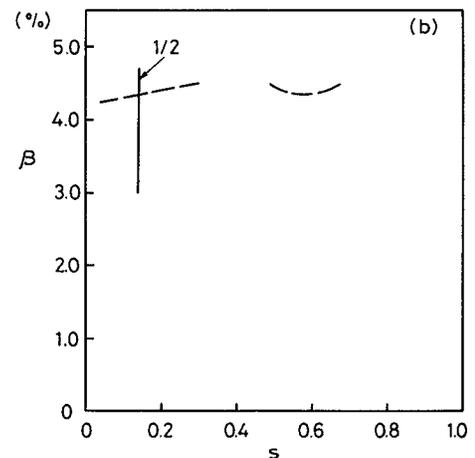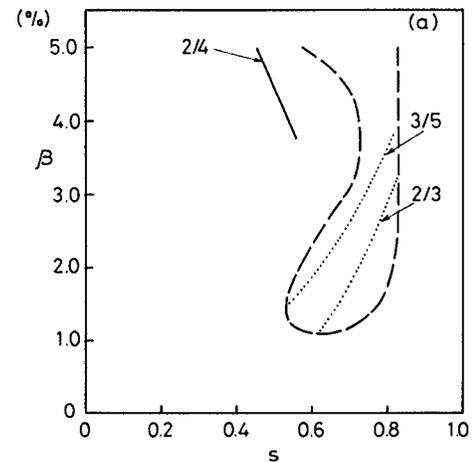

(a)

(b)

FIG. 16. Mercier stability boundary and unstable range of low-n modes as in Fig. 8: (a) obtained with the ATF standard equilibrium with bell-shaped profile and (b) obtained with the ATF standard equilibrium with peaked pressure profile.

FIG. 14. Mercier stability boundary and unstable range of low-n modes, same as in Fig. 8, but for equilibrium E.

boundary calculation for a similar ATF equilibrium.[20] The critical beta value of 3.0% obtained in Fig. 16(b) is similar to that of Cooper et al.,[31] where a critical beta value of 3.5% was obtained by iterating the pressure profile to reach an optimal equilibrium stable to both the Mercier modes and ballooning modes.

In summary, two kinds of low-n modes are found. The first kind is very localized around some rational surface with a single Fourier mode strongly dominating. When a low-n mode of this kind is found to be unstable, the Mercier mode is also unstable at the corresponding rational surface. The critical beta given by the Mercier criterion is always lower than that of a localized low-n mode. The second kind of low-n mode has very global mode structures with multiple helicity. The Mercier criterion cannot adequately describe these types of modes.

B. Discussion

We have shown that gaps exist between the marginal stability boundaries of Mercier modes and those of low-n modes. Recall that we have defined marginal stability of low-n modes to correspond to the point that $-\omega^2/\omega_A^2 = 10^{-4}$. It is of course possible that there exist marginally unstable low-n modes inside these gaps with very small growth rates, as shown by Sugama and Wakatani,[6] for a one-dimensional model. Our fully 3-D results indicate the same feature. Figure 17 shows the growth rate of an $n = 3$ mode as a function of volume-averaged plasma beta β for the equilibrium A. The eigenvalue of a global-type $n = 2$ mode for the ATF equilibrium is also shown for comparison. We see that the growth rate for the localized $n = 3$ mode is very flat near the critical beta value, whereas the growth rate for the global-type $n = 2$ mode is almost a linear function of β. The same tendency was also obseved for other equilibria considered in this paper. Thus, it is reasonable to assert that weakly unstable low-n modes exist near the Mercier marginal stability boundary.

Since the growth rates of Mercier-type low-n modes are largely determined by the values of the Mercier parameter $D_M < 0$, we plot in Fig. 18 the growth rates of an $n = 3$ mode as a function of $-D_M$ evaluated at the rational surface
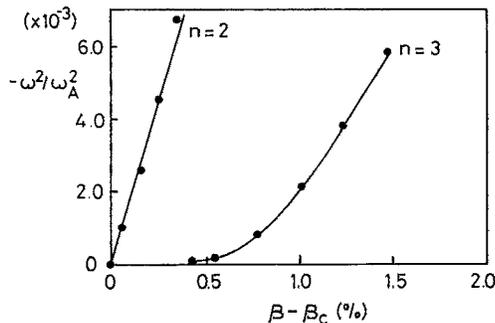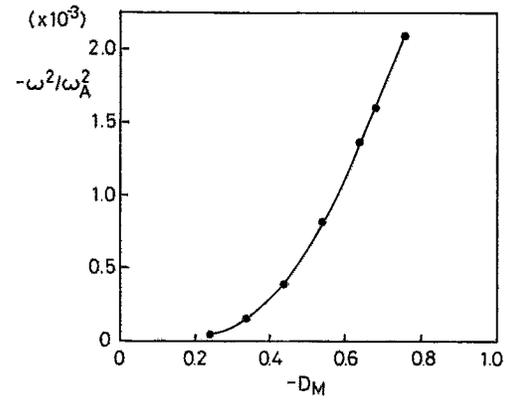

FIG. 18. Eigenvalues of the unstable $n = 3$ mode of equilibrium A versus the Mercier criterion parameter $-D_M$ evaluated at the $\iota = 3/4$ rational flux surface.

$\iota = 3/4$, for the equilibrium A. Again we see that the growth rate is very small and flat near the Mercier marginal limit $-D_M = 0$. The eigenvalue is 10^{-4} for $-D_M = 0.3$. Kulsrud[32] derived an analytic expression for the growth rates of Mercier modes. The growth rate varies as $-\omega^2/\omega_A^2 \propto \exp(-c/\sqrt{-D_M})$ for small $-D_M$, where c is a constant. From this expression, it is evident that the growth rates of low-n modes can be extremely small near the Mercier stability limits $-D_M = 0$. Our fully 3-D results also indicate this tendency.

It is now clear that finite growth rates of localized low-n modes correspond to finite values of the Mercier parameter $-D_M$ at the unstable rational surfaces. In the cases shown in Figs. 13 and 16, where the Mercier modes were unstable but the corresponding low-n modes were either stable or weakly unstable with $-\omega^2/\omega_A^2 < 10^{-4}$, the values of $-D_M$ are found to be relatively small. For the $\iota = 2/3$ surface in Fig. 13, the maximum is $-D_M = 0.14$, and in Fig. 16(a) it is $-D_M = 0.18$ for the $\iota = 2/3$ surface and $-D_M = 0.33$ for the $\iota = 3/5$ surface. In order to quantify the magnitude of $-D_M$ that is required to yield finite growth rates, we plot in Fig. 19 the values of $-D_M$ at which the growth rates are
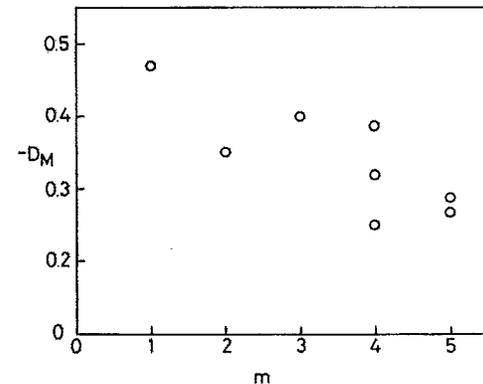

FIG. 17. Eigenvalues of the unstable $n = 3$ mode and $n = 2$ mode obtained with equilibrium A as functions of $\beta - \beta_c$, where β_c denotes the critical beta value of marginal stability for each unstable mode.

FIG. 19. Values of $-D_M$ versus the dominating poloidal mode number m of various low-n instabilities at a fixed growth rate corresponding to $-\omega^2/\omega_A^2 = 10^{-4}$.

$-\omega^2/\omega_A^2 = 10^{-4}$ for the low-n modes studied, as a function of the main poloidal mode number. We see that the value of $-D_M$ varies from 0.25 to 0.47. Therefore, if one can neglect marginally unstable modes with very weak growth rates, the stability limit of localized low-n modes is more accurately modeled with the condition $-D_M \simeq 0.35$ rather than $-D_M = 0$, at least for the torsatron configurations studied here. We note that this full 3-D result is similar to that found by Nakamura et al.[8] using the stellarator expansion approximation.

V. SUMMARY AND CONCLUSIONS

We have extended the TERPSICHORE incompressible 3-D MHD code to incorporate the full ideal MHD model, in order to calculate physical growth rates. The tunable integration method has been implemented and shown to stabilize the numerically unstable continuum modes induced by the finite hybrid method. The new code has been benchmarked and used in the computations in this paper.

We have performed a comprehensive fully 3-D investigation of ideal MHD stability of Mercier modes and nonlocal low-n modes with fixed boundary conditions. The stability of internal low-n modes were compared with those of Mercier modes for $l = 2$ torsatron configurations.

Our results show a definite correlation between the localized low-n modes and the Mercier modes. When the localized low-n modes are found to be unstable, the Mercier modes are also unstable at the corresponding rational magnetic surfaces. On the other hand, when the Mercier criterion indicates instability at some rational surfaces, the corresponding low-n modes can also be considered unstable. More precisely, finite values of the Mercier criterion $-D_M \gtrsim 0.35$ are correlated with unstable low-n modes with finite growth rates $-\omega^2/\omega_A^2 \geqslant 10^{-4}$. Near the Mercier stability limits or $-D_M \lesssim 0.35$, the unstable localized low-n modes tend to have very small growth rates. These marginally unstable modes are likely to be stabilized by various kinetic effects or the presence of magnetic islands neglected in the ideal MHD model.

Another type of low-n mode also exists that is very global radially and displays strong poloidal mode coupling. These global modes tend to concentrate in the region of tokamaklike magnetic shear induced by relatively high beta ($\beta > 2\%$). Their stability cannot be described by the Mercier criterion which applies only to modes localized around a single rational surface. They may be more stable or unstable than Mercier modes. For these internal global modes, a free boundary analysis may yield more restrictive stability limits, as previously demonstrated for the ATF device.[20,24]

We conclude that the stability of both the Mercier mode and low-n modes must be determined in order to have a complete MHD stability picture of a stellarator device. The Mercier criterion can only indicate the stability of low-n modes localized around a single resonant magnetic surface. Three-dimensional nonlocal MHD codes are indispensable tools for computing the stability of global-type low-n modes in stellarator configurations.

[1]V. D. Shafranov, Nucl. Fusion 20, 1075 (1980).
[2]J. L. Johnson, Comput. Phys. Rep. 4, 37 (1986).
[3]B. A. Carreras, G. Grieger, J. H. Harris, J. L. Johnson, J. F. Lyon, O. Motojima, F. Rau, H. Renner, J. A. Rome, K. Uo, M. Wakatani, and H. Wobig, Nucl. Fusion 28, 1613 (1988).
[4]R. Gruber, W. Kerner, P. Merkel, J. N. Nührenberg, W. Schneider, and F. Troyon, Comput. Phys. Commun. 24, 389 (1981).
[5]P. Merkel, J. N. Nührenberg, R. Gruber, and F. Troyon, Nucl. Fusion 23, 1061 (1983).
[6]H. Sugama and M. Wakatani, J. Phys. Soc. Jpn. 58, 1128 (1989).
[7]N. Dominguez, J.-N. Leboeuf, B. A. Carreras, and V. E. Lynch, Nucl. Fusion 29, 2079 (1989).
[8]Y. Nakamura, K. Ichiguchi, M. Wakatani, and J. L. Johnson, J. Phys. Soc. Jpn. 58, 3157 (1989).
[9]C. Mercier, Nucl. Fusion 1, 47 (1960).
[10]R. Gruber, F. Troyon, D. Berger, L. C. Bernard, S. Rousset, R. Shreiber, W. Kerner, W. Schneider, and K. V. Roberts, Comput. Phys. Commun. 21, 323 (1981).
[11]R. Gruber, S. Semenzato, F. Troyon, T. Tsunematsu, W. Kerner, P. Merkel, and W. Schneider, Comput. Phys. Commun. 24, 363 (1981).
[12]J. M. Greene and J. L. Johnson, Phys. Fluids 4, 875 (1961).
[13]L. M. Kovrizhnykh and S. V. Shchepetov, Sov. J. Plasma Phys. 6, 533 (1980).
[14]G. Anania and J. L. Johnson, Phys. Fluids 26, 3070 (1983).
[15]D. V. Anderson, W. A. Cooper, U. Schwenn, and R. Gruber, in Theory of Fusion Plasmas, Proceedings of the Joint Varenna–Lausanne International Workshop, Chexbres, Switzerland, 1988 (Editrice Compositori, Bologna, Italy, 1989), p. 93.
[16]U. Schwenn, D. V. Anderson, W. A. Cooper, R. Gruber, and S. Merazzi, in Controlled Fusion and Plasma Heating, Proceedings of the 17th European Conference, Amsterdam, The Netherlands (European Physical Society, Petit-Lancy, 1990), Vol. 14B, Part II, p. 931.
[17]W. A. Cooper, G. Y. Fu, R. Gruber, S. Merazzi, U. Schwenn, and D. V. Anderson, in Theory of Fusion Plasmas, Proceedings of the Joint Varenna–Lausanne International Workshop, Valla Monastero, Varenna, Italy, 1990 (Editrice Compositori, Bologna, Italy, 1990), p. 655.
[18]C. Schwab, in Ref. 15, p. 85.
[19]C. Schwab, in Ref. 17, p. 667.
[20]W. A. Cooper, G. Y. Fu, R. Gruber, C. Schwab, U. Schwenn, S. Merazzi, and D. V. Anderson, in Plasma Physics and Controlled Nuclear Fusion Research, 1990 (IAEA, Vienna, 1991), Vol. 2, p. 193.
[21]S. P. Hirshman and J. C. Whitson, Phys. Fluids 26, 3553 (1983).
[22]S. P. Hirshman, W. I. Van Rij, and P. Merkel, Comput. Phys. Commun. 43, 143 (1986).
[23]A. H. Boozer, Phys. Fluids 23, 904 (1980).
[24]G. Rewoldt and J. L. Johnson, Nucl. Fusion 24, 733 (1984).
[25]L. S. Solov'ev, Zh. Tekh. Fiz. 53, 626 (1967) [Sov. Phys. JETP 26, 400 (1968)].
[26]A. Bondeson, G. Vlad, and H. Lütjens, in Ref. 16, p. 906.
[27]F. Herrnegger, P. Merkel, and J. L. Johnson, J. Comput. Phys. 66, 445 (1986).
[28]A. Bondeson and G. Y. Fu, Comput. Phys. Commun. 66, 167 (1991).
[29]F. Bauer, O. Betancourt, and P. Garabedian, Magnetohydrodynamic Equilibrium and Stability of Stellarators (Springer-Verlag, New York, 1984).
[30]J. F. Lyon, B. A. Carreras, K. K. Chipley, M. J. Cole, J. H. Harris, T. C. Jernigan, R. L. Johnson, V. E. Lynch, B. E. Nelson, J. A. Rome, J. Sheffield, and P. B. Thompson, Fusion Technol. 10, 179 (1986).
[31]W. A. Cooper, S. P. Hirshman, and D. K. Lee, Nucl. Fusion 29, 617 (1989).
[32]R. M. Kulsrud, Phys. Fluids 6, 904 (1963).